Mon. Not. R. Astron. Soc. **000**, 000–000 (0000) Printed 1 February 2008 (MN LATEX style file v1.4)

Cosmological model differentiation through weak gravitational lensing

Antonio C. C. Guimarães
Department of Physics, Brown University, Providence, RI 02912, USA; guimar@het.brown.edu

27-Feb-2002, BROWN-HET-1291, astro-ph/0202507

ABSTRACT
We investigate the potential of weak gravitational lensing maps to differentiate between distinct cosmological models, considering cosmic variance due to a limited map extension and the presence of noise. We introduce a measure of the differentiation between two models under a chosen lensing statistics. That enables one to determine in which circumstances (map size and noise level), and for which lensing measures two models can be differentiated at a desired confidence level. As an application, we simulate convergence maps for three cosmological models (SCDM, OCDM, and ΛCDM), calculate several lensing analyses for them, and compute the differentiation between the models under these analyses. We use first, second, and higher order statistics, including Minkowski functionals, which provide a complete morphological characterization of the lensing maps. We examine for each lensing measure used how noise affects its description of the convergence, and how this affects its ability to differentiate between cosmological models. Our results corroborate to the valuable use of weak gravitational lensing as a cosmological tool.

Key words: gravitational lensing — large-scale structure of universe

1 INTRODUCTION

The mass inhomogeneities in the Universe leave an imprint in the light traveling through it: that is gravitational lensing. The retrieval of this information can be of singular value to narrow down cosmological models.

The statistical shape distortion of distant galaxies, or cosmic shear, is is one of the aspects of gravitational lensing in the weak regime (small deflection angles), and has been observed by several groups (see Mellier 1999 for a review up to this year, and for more recent measurements see Van Waerbeke et al. 2000; Wittman et al. 2000; Fischer et al. 2000; Bacon, Refregier & Ellis 2000; Kaiser, Wilson & Luppino 2000; Maoli et al. 2001; Rhodes, Refregier & Groth 2001; Van Waerbeke et al. 2001; Hoekstra, Yee & Gladders 2001). Concomitantly, theoretical works in the area indicated that such measurements can be very revealing about the large-scale structure of the universe (Kaiser & Squires 1993; Bernardeau, Van Waerbeke & Mellier 1997; Jain, Seljak & White 2000; Bartelmann & Schneider 1999, 2001), in addition to the study of individual galaxy clusters. The main attractive of gravitational lensing being that it probes mass directly, avoiding issues such as mass-light bias.

The perspective of a growing number and quality of weak lensing measurements stimulates the question of how far the use of weak gravitational lensing as an astrophysical and cosmological tool can go, and how much can be achieved. That ultimately depends on the extension and quality of the lensing maps, the amount of information that can be extracted from them, and the ability of this information to differentiate between theoretical models.

The aim of this paper is to investigate the potential of weak gravitational lensing maps to differentiate between different cosmological models. We incorporate limitations resulting from the presence of noise and cosmic variance for several lensing measures, including a morphological analysis, the Minkowski functionals (Matsubara & Jain 2001; Sato et al. 2001).

Theoretical predictions for lensing measures can be obtained by two approaches. The first is the analytical, which is based on gravitational lens theory, and resorts frequently on perturbation theory to calculate expressions for various statistics in an assumed model. The second approach is to simulate realizations of lensing maps in a chosen model, and directly measure the quantities of choice. Here we review the first, and use the second for an application example.

We obtain that even for modest field sizes (9 degrees^2), and noise at the level of current surveys, the cluster normalized cold dark matter models (SCDM, OCDM, and ΛCDM) can be differentiated with significant confidence. Second order statistics (convergence variance and lensing measures dependent on it) proved to be the best discriminatory analyses for these models. However, we also obtain that higher order statistics (measures that are sensitive to non-Gaussian features of lensing maps) can differentiate between some models in certain circumstances. This result is particularly important when aiming to differentiate

cosmological models that have the same power spectrum, but distinct non-Gaussian properties. We suggest that Minkowski functionals should be included in the row of statistics normally used to extract information from lensing maps, because their morphological characterization of maps contains information that is independent of measures such as the probability distribution function of the convergence.

The paper is organized as the following. In Section 2 we briefly review how lensing maps can be generated and analyzed, and we introduce a measure of the differentiation between two models through a chosen lensing statistic. In Section 3 we compare three cosmological models (SCDM, OCDM, and ΛCDM) as saw through weak gravitational lensing. Our conclusions are in Section 4.

2 LENSING MAP

2.1 Generation

The image distortion of background galaxies by weak gravitational lensing can be expressed by the distortion matrix (Bartelmann & Schneider 2001)

$$\mathcal{A}(\boldsymbol{\theta}) = \begin{pmatrix} 1-\kappa-\gamma_1 & -\gamma_2 \\ -\gamma_2 & 1-\kappa+\gamma_1 \end{pmatrix} , \tag{1}$$

where κ is called the convergence, and $\gamma \equiv \gamma_1 + i\gamma_2 = |\gamma|e^{2i\varphi}$ is the shear.

Matrix $\mathcal{A}$ transforms a circular source image in an ellipse with semi-axis stretched by a factor $(1-\kappa \pm |\gamma|)^{-1}$ from the original radius, and magnification $\mu = (\det\mathcal{A})^{-1} = [(1-\kappa)^2 - \gamma^2)]^{-1}$.

The shear can be directly estimated from ellipticity measurements of background galaxies, and shear and convergence can be mapped in each other through

$$\gamma(\boldsymbol{\theta}) = \frac{1}{\pi}\int \mathcal{W}(\boldsymbol{\theta}-\boldsymbol{\theta}')\kappa(\boldsymbol{\theta}')d^2\boldsymbol{\theta}' , \tag{2}$$

with

$$\mathcal{W}(\boldsymbol{\theta}) = \frac{-1}{(\theta_1 - i\theta_2)^2} , \tag{3}$$

or through the relation between their Fourier transforms

$$\tilde{\kappa}(\boldsymbol{l}) = \frac{l_1^2 - l_2^2}{l^2}\tilde{\gamma}_1(\boldsymbol{l}) + \frac{2l_1l_2}{l^2}\tilde{\gamma}_2(\boldsymbol{l}) . \tag{4}$$

We can compute the components $\mathcal{A}_{ij}$ of the distortion matrix by calculating the angular deflection of a photon traveling from a comoving distance w through a gravitational potential Φ

$$\mathcal{A}_{ij}(\boldsymbol{\theta}) = -2\int_0^w g(w',w)\partial_i\partial_j\Phi(\boldsymbol{\theta},w')dw' , \tag{5}$$

where

$$g(w',w) = \frac{f_K(w')f_K(w-w')}{f_K(w)} , \tag{6}$$

and $f_K(w)$ is the curvature-dependent comoving angular diameter distance.

From equation (5) and using Poisson equation,

$$\nabla^2\Phi = \frac{3}{2}H_o^2\Omega_m\frac{\delta}{a} , \tag{7}$$

where δ is the density contrast and a is the scale factor, we can write the convergence as

$$\kappa(\boldsymbol{\theta}) = \frac{3H_o^2}{2}\Omega_m\int_0^w g(w',w)\frac{\delta(\boldsymbol{\theta},w')}{a(w')}dw' . \tag{8}$$

The convergence is a weighted projection of the mass inhomogeneities between source and observer.

In this work we concentrate on the convergence field $\kappa(\boldsymbol{\theta})$ as our lensing map. It can be derived from a real or simulated shear map through equation (4), or computed directly from a N-body simulation of $\delta(\boldsymbol{\theta},w)$ and the use of equation (8). We choose the second approach for our application example at Section 3.

2.2 Statistics

Here we review some statistics used to characterize the convergence field, the angular power spectrum, second and higher order statistics, the probability distribution function (PDF), and Minkowski functionals.

The convergence field can be expanded in Fourier modes, and their amplitude averaged for each wavelength. That is the direct calculation of the angular power spectrum of the convergence from a real or simulated lensing map,

$$P_\kappa(l) \equiv \langle |\tilde{\kappa}(\boldsymbol{l})|^2 \rangle \ . \tag{9}$$

An analytical prediction for the convergence angular power spectrum can be obtained from equation (8), and be expressed as a weighted integral of the time-evolving density power spectrum $P_\delta(k,w)$

$$2\pi l^2 P_\kappa(l) = 36\pi^2 \Omega_m^2 l^2 \int_0^{w_o} \frac{g^2(w,w_o)}{f_K^2(w)} a^{-2}(w) P_\delta \left[k = \frac{l}{f_K(w)}, w \right] dw \ . \tag{10}$$

However, the angular power spectrum does not contain all the statistical information about the κ-map. All the information in the phases of the complex Fourier modes is lost. These phases carry the non-Gaussian features of the map, which are important signatures of non-linear evolution, and also of models of structure formation containing non-Gaussian initial conditions (as opposed to most of the inflationary scenarios).

The Fourier transform of the angular power spectrum of the convergence is the angular two-point correlation function $C_\kappa(r) = \langle \kappa(\boldsymbol{\theta}) \kappa(\boldsymbol{\theta} + \boldsymbol{r}) \rangle$. The convergence field variance $\sigma_\kappa^2 \equiv \langle \kappa^2 \rangle$ can be seen as the value of the angular two-point correlation function at the origin, $\sigma_\kappa^2 = C_\kappa(0)$, and expressed as (Jain & Seljak 1997; Bernardeau, Van Waerbeke & Mellier 1997)

$$\langle \kappa^2 \rangle = 36\pi^2 \Omega_m^2 \int_0^\infty k dk \int_0^{w_o} \frac{g^2(w)}{a^2(w)} P_\delta \left(k, w\right) W_2^2 \left[k f_K(w) \theta_s\right] dw \ , \tag{11}$$

where $W_2 = 2J_1(x)/x$ is the Fourier transform of the top-hat window function (J_1 is the Bessel function of first order). Expressions for higher order powers, $\langle \kappa^3 \rangle$ and $\langle \kappa^4 \rangle$, can be similarly obtained as integrals of the bispectrum and trispectrum, respectively. See Hui (1999), and Munshi & Jain (2000), or Cooray & Hu (2001) for more elegant expressions. Related statistics are the skewness $S = \langle \kappa^3 \rangle / \sigma_\kappa^3$, the kurtosis $K = (\langle \kappa^4 \rangle / \sigma_\kappa^4) - 3$, or the more general moments $S_N = \langle \kappa^N \rangle / \sigma_\kappa^{2(N-1)}$.

The probability distribution function contains in principle more information than the variance and higher order moments of the convergence field taken individually, which can be calculated from the PDF itself,

$$\langle \kappa^N \rangle = \int F(\kappa) \kappa^N d\kappa \ . \tag{12}$$

The PDF can be expanded around a Gaussian through the Edgeworth approximation (Jusziewicz el al. 1995)

$$F(\kappa) = \frac{e^{-\kappa^2/2\sigma_\kappa^2}}{\sqrt{2\pi}\,\sigma_\kappa} \left\{ 1 + \sigma_\kappa \frac{S_3}{3!} \mathrm{H}_3(\kappa/\sigma_\kappa) + \sigma_\kappa^2 \left[\frac{S_4}{4!} \mathrm{H}_4(\kappa/\sigma_\kappa) + \frac{S_3^2}{6!} \mathrm{H}_6(\kappa/\sigma_\kappa) \right] + ... \right\} \ , \tag{13}$$

where H_η is the Hermite polynomial of order η.

Minkowski functionals contain all the morphological information about a convex body, and for a Gaussian field they can be calculated exactly (Winitzki & Kosowsky 1998). That makes the Minkowski functionals of the convergence maps a very interesting statistic to use (Matsubara & Jain 2001; Sato et al. 2001). A threshold value ν defines excursion sets in which the value of $\nu(\boldsymbol{\theta}) \equiv \kappa(\boldsymbol{\theta})/\sigma_\kappa$ is larger than the threshold: $v_0(\nu)$ is the fractional area of the map above the threshold, $v_1(\nu)$ the boundary length (per area), and $v_2(\nu)$ the Euler characteristic. This last functional is equivalent to the topological genus of the map, roughly speaking, the number of disconnected regions minus the number of holes.

Approximate expressions for the Minkowski functionals can be obtained through perturbation theory about the exact expressions for a Gaussian field (Matsubara 2000)

$$v_0(\nu) \approx \frac{1}{2}\mathrm{erfc}\left(\frac{\nu}{\sqrt{2}}\right) + \frac{1}{6\sqrt{2\pi}} e^{-\nu^2/2} \sigma_\kappa S_3^{(0)} \mathrm{H}_2(\nu) \ , \tag{14}$$

$$v_1(\nu) \approx \frac{1}{8\sqrt{2}} \frac{\sigma_1}{\sigma_\kappa} \mathrm{e}^{-\nu^2/2} \left\{ 1 + \sigma_\kappa \left[\frac{S_3^{(0)}}{6} \mathrm{H}_3(\nu) + \frac{S_3^{(1)}}{3} \mathrm{H}_1(\nu) \right] \right\} \ , \tag{15}$$

$$v_2(\nu) \approx \frac{1}{2(2\pi)^{\frac{3}{2}}} \frac{\sigma_1^2}{\sigma_\kappa^2} \mathrm{e}^{-\nu^2/2} \left\{ \mathrm{H}_1(\nu) + \sigma_\kappa \left[\frac{S_3^{(0)}}{6} \mathrm{H}_4(\nu) + \frac{2S_3^{(1)}}{3} \mathrm{H}_2(\nu) + \frac{S_3^{(2)}}{3} \right] \right\} \ , \tag{16}$$

where $\sigma_1^2 \equiv \langle (\nabla\kappa)^2 \rangle$, and skewness parameters are defined by $S_3^{(0)} \equiv \langle \kappa^3 \rangle / \sigma_\kappa^4$, $S_3^{(1)} \equiv -(3/4) \langle \kappa^2 (\nabla^2 \kappa) \rangle / (\sigma_\kappa^2 \sigma_1^2)$ and $S_3^{(2)} \equiv -3 \langle (\nabla\kappa \cdot \nabla\kappa)(\nabla^2\kappa) \rangle / \sigma_1^4$.

2.3 Differentiation

Here we introduce a measure aimed to quantify the difference between two models, or a model and an observational result, under a chosen lensing map analysis (Guimarães 2001). This quantity is also aimed to allow the comparison of different lensing statistics, for instance, being able to point which analysis is the most appropriate to use when trying to differentiate between models through weak lensing. We construct one such quantity in Appendix A.

The *differentiation* $\mathcal{D}$ between models A and B under the lensing analysis Y is defined as

$$\mathcal{D}[Y] \equiv 1 - e^{-\chi^2/2} \ , \tag{17}$$

where

Figure 1. Convergence maps for SCDM (left), ΛCDM (center), and OCDM (right). The top maps are pure (no noise added), and the bottom maps have noise added. All maps are 3×3 degrees^2, and smoothed at 1 arcmin.

Table 1. Cosmological models considered. Other parameters: $h = 0.7$, $\Gamma = \Omega_m h$, $\Omega_b = 0$, $L_{box} = 128h^{-1}Mpc$, $l_{soft} = 30h^{-1}kpc$, $N_{part} = 128^3$.

	Ω_m	Ω_Λ	σ_8
SCDM	1.0	0	0.56
OCDM	0.3	0	0.84
ΛCDM	0.3	0.7	0.99

$$\chi^2 \equiv \frac{1}{N}\sum_i^N \frac{[\bar{Y}_A(p_i) - \bar{Y}_B(p_i)]^2}{\sigma_A^2(p_i) + \sigma_B^2(p_i)} \ . \tag{18}$$

$\bar{Y}_A(p_i)$ is the mean value of the lensing measure Y for model A at N values of the analysis parameter p, and its variance is $\sigma_A^2(p_i)$. Equivalently for model B. Equation (18) is a particular discrete form of the more general expression (A11), when the parameter interval is divided in N equal-size segments.

According to this definition, the differentiation is quantified on a scale from 0 to 1. For models that are similar under a given analysis $\mathcal{D}[Y] \approx 0$, and for very distinct models $\mathcal{D}[Y] \approx 1$. If one wants to study a set of models, it is desirable to find which lensing measures give the largest differentiations, so the discrimination between models is robust. On the other hand, if one has an observational result, the interest is to find which model gives the lowest differentiation for the chosen analysis. That is the best fit model.

If we assume that the differentiation has a Gaussian distribution, then it follows that its variance is

$$\Delta^2[\mathcal{D}] = \chi^2 e^{-\chi^2} \ . \tag{19}$$

3 STUDY OF WEAK LENSING MAPS

3.1 Map construction

We compare three important cosmological models, SCDM, OCDM, and ΛCDM (see table 1). We used the Hydra N-body code (Couchman, Thomas & Pearce, 1995) to simulate the large-scale mass distribution in these models by evolving 128^3 particles from a redshift $z = 50$ to $z = 0$. The particle coordinates at juxtaposed boxes from a redshift $z = 1$ (our assumed source redshift) to $z = 0$ were saved, and projected into a middle plane in each box (the orientation and origin of the projections were randomized). The resulting set of 2D density contrast fields (in 1024^2 grids) at those positions in redshift space were used as a discrete approximation for the computation of the convergence field according to equation (8), that is usually refered to as multiple-plane lens method.

The main source of noise in real lensing maps is the intrinsic ellipticities of the background galaxies. We simulated this noise by adding a Gaussian random field to the pure convergence following Van Waerbeke (2000), which showed that this is a good approximation. We then used a top-hat window of radius θ_s to smooth the map, which can be described by

$$\kappa(\boldsymbol{\theta}) = \kappa_o(\boldsymbol{\theta}) + n(\boldsymbol{\theta}) \ , \tag{20}$$

where $\kappa_0(\boldsymbol{\theta})$ is the smoothed pure convergence, and $n(\boldsymbol{\theta})$ is the smoothed noise field. The noise part is a Gaussian correlated field of variance σ_n^2,

$$\sigma_n^2 = \frac{\sigma_\epsilon^2}{2n_g\pi\theta_s^2} \ , \tag{21}$$

where $\sigma_\epsilon^2 = 0.16$ was the intrinsic ellipticity variance adopted, and $n_g = 60$ arcmin^{-2} was the mean source galaxy density assumed. The top-hat smoothing of the original Gaussian random field introduces correlations in the noise at scales bellow twice the smoothing radius.

Figure 1 shows some realizations of the κ-maps. We generated 25 realizations for each model, however, because we only used one N-body simulation for each model, the κ-maps generated cannot be considered to be totally independent. That is not a source of major concern for our objectives in this work.

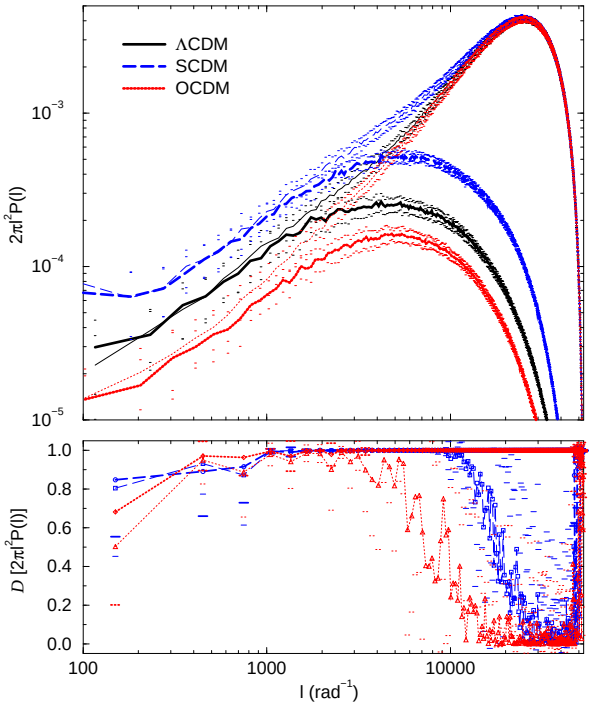

Figure 2. Top panel: angular power spectrum of the convergence field smoothed at 0.25 arcmin scale. Bottom panel: angular power differentiation between models ΛCDM-SCDM (dashed lines), and ΛCDM-OCDM (dotted lines). Thick lines are for pure maps, and thin lines for noisy maps. Only the error-bar tips are show for clarity.

3.2 Statistics and differentiation results

We applied a number of statistical measures to the convergence maps of the three cosmological models. We considered pure (no noise) and noisy maps of field sizes 3×3 degrees^2, and 1×1 degree^2. For each analysis we calculated the differentiation $\mathcal{D}$ according to equation (17) between ΛCDM and SCDM, and between ΛCDM and OCDM.

Figure 2 shows the results for the angular power spectrum of the convergence for a field smoothed with $\theta_s = 0.25$ arcmin, and its differentiation between models. The total power of the convergence field, P_κ, is just given by the sum of the power of the pure field P_{κ_o} and the power of the noise field P_n (a power law), because the two fields are uncorrelated (by construction),

$$P_\kappa(l) = P_{\kappa_o}(l) + P_n(l)\ , \tag{22}$$

and its variance can also be fragmented as

$$\Delta^2[P_\kappa] = \Delta^2[P_{\kappa_o}] + \Delta^2[P_n] + \Delta^2[\langle\tilde{\kappa}_o\tilde{n}^*\rangle] + \Delta^2[\langle\tilde{\kappa}_o^*\tilde{n}\rangle]\ . \tag{23}$$

For low values of the wavenumber l (large scales) noise gives a small contribution to the power of the convergence, but the variance of the measured power is large due to the restricted sampling. This large variance implies a lower differentiation between models at low l. For high l (small scales) the measured power is suppressed by the field smoothing at wavenumber values above $l_s \sim \theta_s^{-1}$. The noise field gives a major contribution to the total power and power variance, such that the examined models become indistinguishable as quantified by the low values of $\mathcal{D}\,[2\pi l^2 P(l)]$ in this case. Note that the analyzed maps have different areas (ΛCDM 9.6 degrees^2, SCDM 15.6 degrees^2, and OCDM 12.3 degrees^2), therefore the power variances cannot be directly compared.

The addition of noise transforms the probability distribution function for the pure convergence field F_{κ_o} according to the convolution

$$F_\kappa(x) = \int_{-\infty}^{+\infty} F_{\kappa_o}(y)\frac{e^{(x-y)^2/\sigma_n^2}}{\sqrt{2\pi}\sigma_n}dy\ . \tag{24}$$

For a small smoothing angle θ_s the noise variance σ_n^2 is large, so the convolution has a large effect on the pure convergence PDF. In contrast, for a large θ_s, σ_n^2 is small, and F_κ does not differ substantially from F_{κ_o}. This effect is illustrated on Figure 3, which shows the results for the probability distribution function of the κ field, and the integrated PDF differentiation in the interval $-0.04 < \kappa < 0.04$. The differentiation curves indicate that noise reduces the differentiation between models, but moderately. Smoothing has a much more visible role in reducing this differentiation - the convergence maps for different models are made more homogeneous by smoothing, and therefore made more alike. The map size also has a major effect on

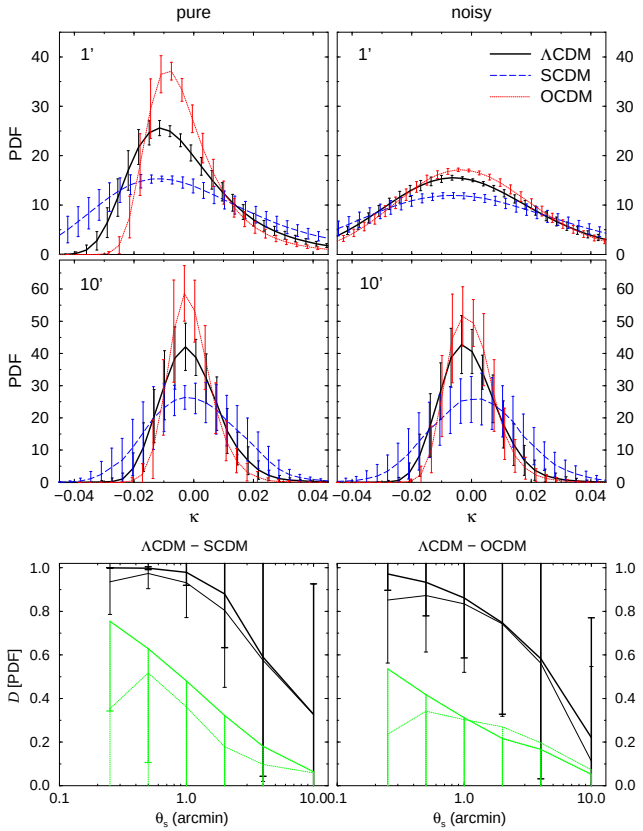

Figure 3. Top panels: convergence probability distribution function for pure (left) and noisy (right) maps at 1 and 10 arcmin smoothing scales of 3×3 degrees^2 fields. Bottom panels: PDF differentiation between ΛCDM-SCDM (bottom left) and ΛCDM-OCDM (bottom right), as function of the smoothing angle θ_s. Thick lines are for pure maps, and thin lines for noisy maps; solid lines are for 3×3 degrees^2 fields, and dotted lines are for 1×1 degree^2 fields (the superior error-bars for these are not show for clarity).

the ability of the PDF analysis to differentiate between models, because the variance of the PDF measurement increases with a reduced field size.

Figure 4 shows the convergence variance $\langle\kappa^2\rangle$ as a function of the smoothing angle, and its model differentiation. Because the pure convergence and noise fields are uncorrelated, the convergence variance can be written as

$$\langle\kappa^2\rangle = \langle\kappa_o^2\rangle + \sigma_n^2 \,, \tag{25}$$

$$\Delta^2[\sigma_\kappa^2] = \Delta^2[\sigma_{\kappa_o}^2] + \Delta^2[\sigma_n^2] + 2\Delta^2[\langle\kappa_o n\rangle] \,. \tag{26}$$

Noise dominates for small field smoothing, because $\sigma_n^2 \propto \theta_s^{-2}$, while the variance of the pure field decreases with a smaller power ($\sigma_{\kappa_0}^2 \sim \theta_s^{-0.8}$), and is negligible for large θ_s (error-bars are increased though). The curves for $\mathcal{D}\left[\langle\kappa^2\rangle\right]$ demonstrates that the field variance is a powerful analysis to discriminate between the models considered, even for small maps.

The mean third power of the field is a direct measure of its deviation from Gaussianity, and its value is not affected by the noise field (see Figure 5), because $\langle n\rangle = \langle n^3\rangle = 0$,

$$\langle\kappa^3\rangle = \langle\kappa_o^3\rangle \,. \tag{27}$$

Unfortunately the noise field increases $\langle\kappa^3\rangle$ error-bars, reducing the differentiation between models

$$\Delta^2[\langle\kappa^3\rangle] = \Delta^2[\langle\kappa_o^3\rangle] + \Delta^2[\langle n^3\rangle] + 2\Delta^2[\langle\kappa_o^2 n\rangle] + 2\Delta^2[\langle\kappa_o n^2\rangle] \,. \tag{28}$$

Figure 5 also shows the results for the related quantity skewness, $S = \langle\kappa^3\rangle/\sigma_\kappa^3$. Its null differentiation between ΛCDM and OCDM, and not null between ΛCDM and SCDM, suggests that the convergence skewness is sensitive to the mass density, and insensitive to the cosmological constant.

Figure 6 shows the results for the mean fourth power of the convergence field $\langle\kappa^4\rangle$, and kurtosis $K = (\langle\kappa^4\rangle/\sigma_\kappa^4) - 3$. The contribution of the noise field can be visualized in the expression

$$\langle\kappa^4\rangle = \langle\kappa_o^4\rangle + \langle n^4\rangle + 6\langle\kappa_o^2 n^2\rangle \,, \tag{29}$$

where $\langle n^4\rangle = 3\sigma_n^4$. This coupling of the pure field with the noise field, $\langle\kappa_o^2 n^2\rangle$ term, allows the model differentiation for $\langle\kappa^4\rangle$ to be larger for the noisy maps than for the pure ones. The kurtosis of Gaussian fields is null, and that is what is observed for

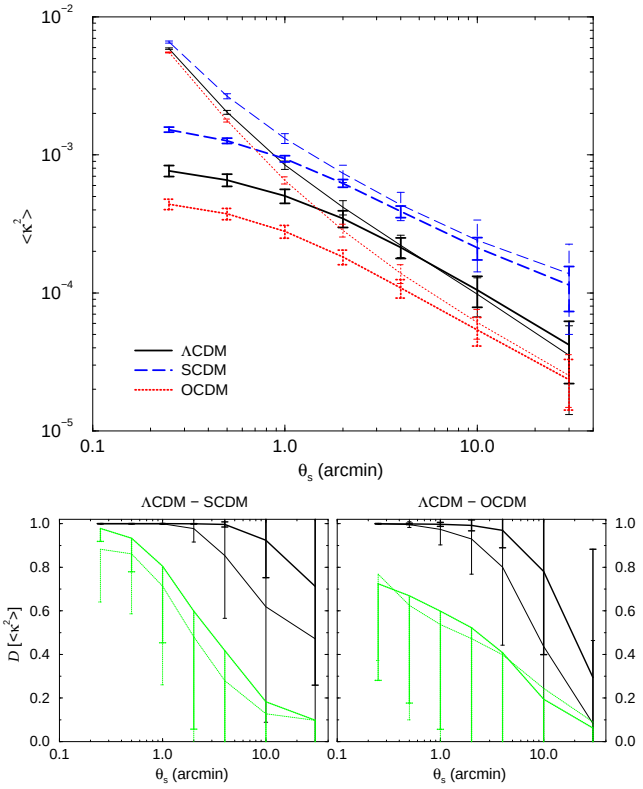

Figure 4. Convergence variance of 3×3 degrees^2 fields (top panel), and convergence variance differentiation between ΛCDM-SCDM (bottom left) and ΛCDM-OCDM (bottom right), as function of the smoothing angle θ_s. Thick lines are for pure maps, and thin lines for noisy maps. In the bottom panels solid lines are for 3×3 degrees^2 fields, and dotted lines are for 1×1 degree^2 fields (the superior error-bars for these are not show for clarity).

noisy convergence maps at small and large smoothing angles. At small θ_s because noise dominates, and at large θ_s because of the extreme field smoothing.

Some Minkowski functionals curves for the convergence field are shown at Figure 7, and the differentiation results for this analysis of the models are shown at Figure 8. Minkowski functionals are very sensitive to noise and smoothing. The morphology of the convergence maps for the examined models seem to not differ greatly as described by the functionals. However for noisy fields the second and third functionals have considerable discriminatory power at small smoothing angles. It is in principle counter-intuitive that noisy maps would have a larger differentiation than pure convergence maps, but as seen in the case of the $\langle\kappa^4\rangle$ analysis, noise can introduce a "statistical contaminant". The discussion on Minkowski functionals of noisy maps presented in Appendix B may be useful in understanding this effect.

Another interesting result to note is the low differentiation between models under the first Minkowski functional analysis (fractional area), which can be saw as a cumulative PDF. Figure 3 shows a strong differentiation between models under the PDF analysis, so the results for $\mathcal{D}[v_0]$ could seem contradictory with those for $\mathcal{D}[PDF]$, however when we remember that Minkowski functionals are displayed as functions of the threshold $\nu = \kappa/\sigma_\kappa$ this apparent discrepancy disappears. This observation suggests that the large PDF differentiation between the models is due primarily to their very distinct convergence variances.

4 CONCLUSIONS

We study the potential of weak gravitational lensing maps to differentiate between different cosmological models, using a variety of statistical measures, including morphological analysis, and taking in account the effects of noise and the uncertainties resulting from a limited field size.

We reviewed how gravitational lensing maps can be generated, and also revisited some statistics that can be used to characterize the lensing maps, or extract information from them. We introduced the quantity $\mathcal{D}$, which quantifies the differentiation between two sets of lensing maps under a given statistic. We used simulations of convergence maps in three cosmological models (ΛCDM, SCDM, and OCDM) to study and compare these models. Several of the analyses considered here were also investigated in previous works, with results consistent with ours. The novelties presented in this paper are the quantitative description of the differentiation between models (which proved to be very useful), the possibility to compare

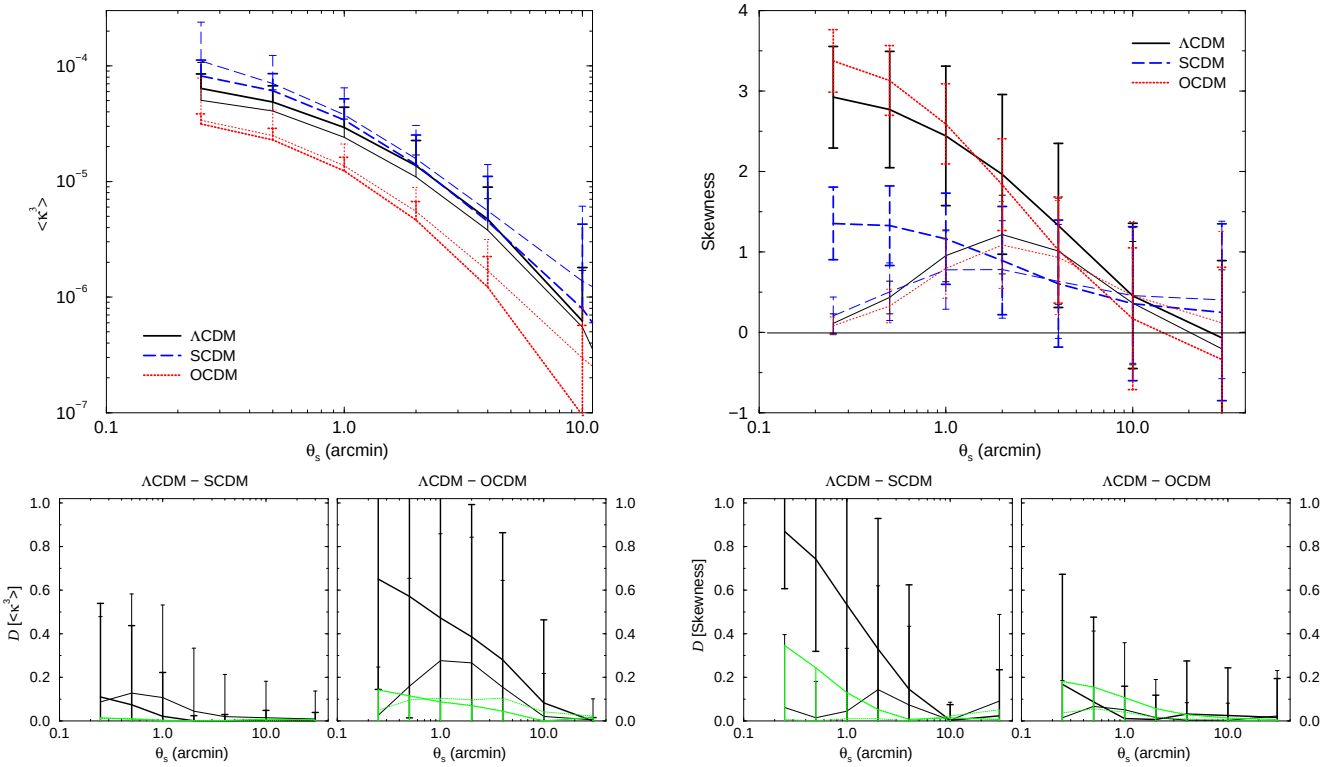

Figure 5. Convergence mean third power (left) and skewness (right). Equal graphic conventions to figure 4 are used.

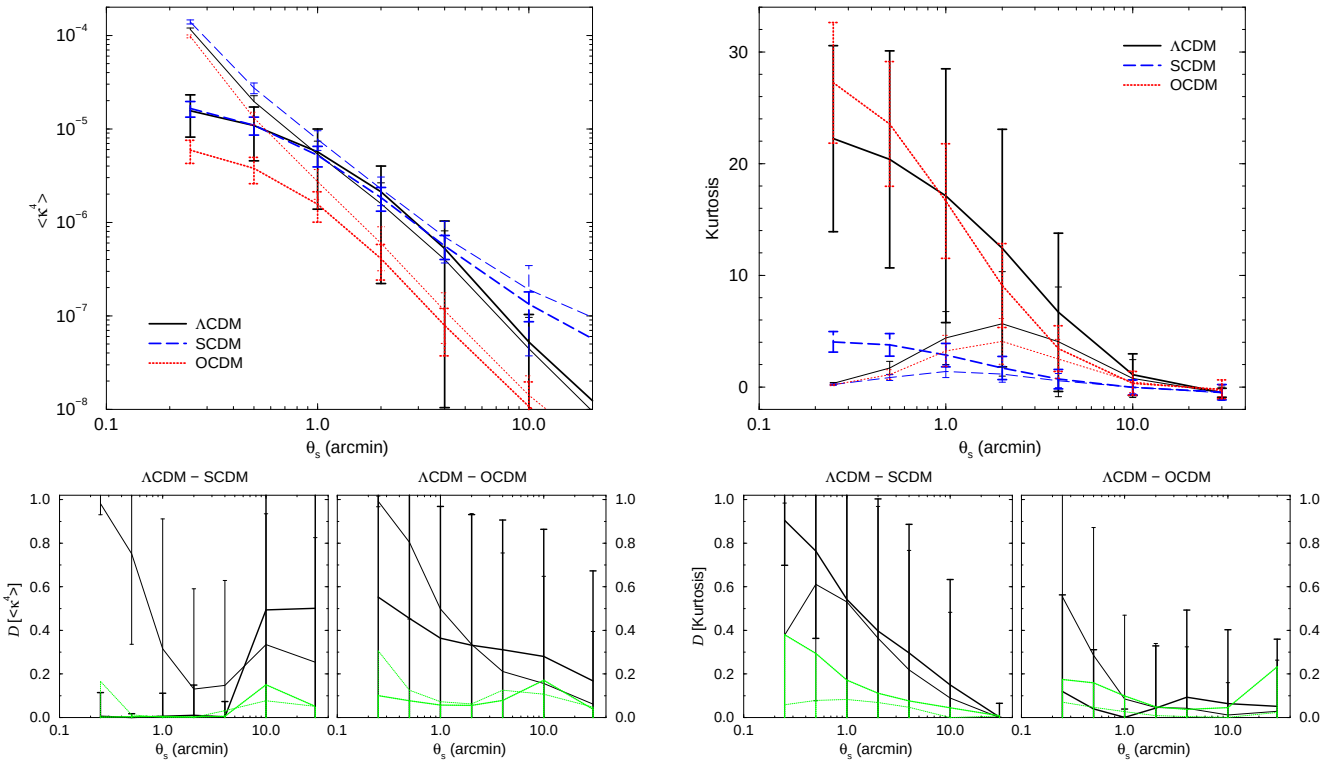

Figure 6. Convergence mean fourth power (left) and kurtosis (right). Equal graphic conventions to figure 4 are used.

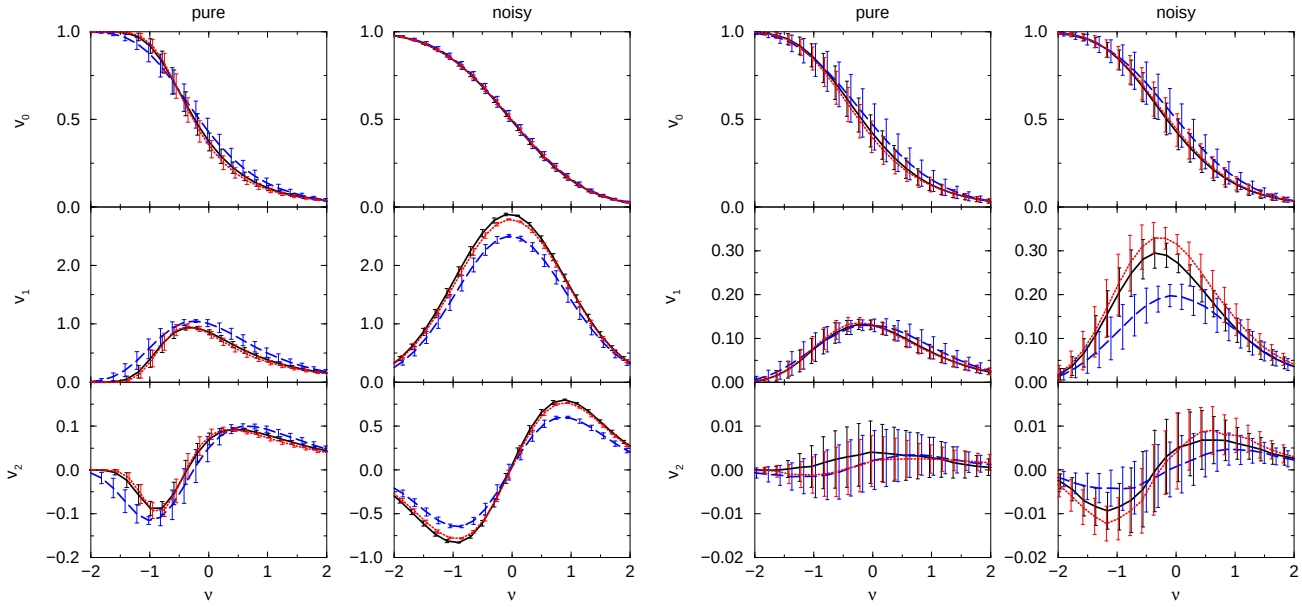

Figure 7. Minkowski functionals for the convergence field (pure and noisy), for smoothing angles 0.25 (left) and 4 (right) arcmin. The first functional v_0 is dimensionless, v_1 units are arcmin^{-1}, and v_2 arcmin^{-2}.

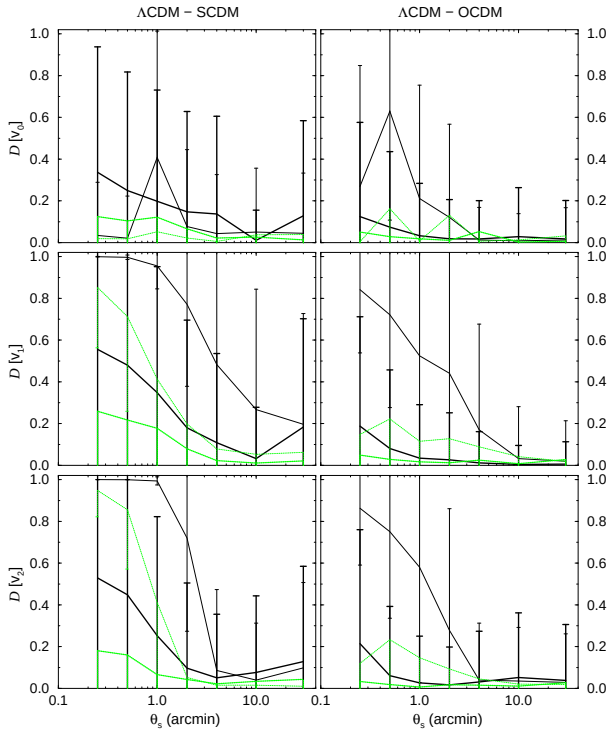

Figure 8. Minkowski functional differentiation between ΛCDM-SCDM (left) and ΛCDM-OCDM (right), as function of the smoothing angle θ_s. Thick lines are for pure maps, and thin lines for noisy maps; solid lines are for 3×3 degrees^2 fields, and dotted lines for 1×1 degree^2 fields (the superior error-bars for these are not show for clarity).

side-by-side different statistics, and a systematic consideration of the role of noise and field size in all lensing measures. It was also the first time that the Minkowski functionals for noisy maps were calculated.

Our results show, as expected, that the lensing measures of small fields have large variance, because of limited sampling. These large variances imply a small value for the differentiation $\mathcal{D}$: the observation of a too small sky patch does not allow the discrimination of cosmological models. Other general behavior, independent of the analysis or model considered, is the approximation of the differentiation values obtained for pure and noisy convergence maps when the smoothing angle is large. As smoothing increases the noise variance decreases (noise becomes irrelevant for a sufficiently high smoothing angle), but

the pure convergence is also homogenized, and the differentiation between models becomes small. Our results suggest that it is advantageous for model discrimination purposes to use a minimum smoothing, even considering that this implies a noisier map.

For purposes of discriminating the three models examined in our simulations, the variance and the angular power spectrum of the convergence (two of the most simple and popular analysis) proved to be very good lensing measures. Even for small field sizes, and noisy maps, the convergence variance can differentiate between the models at a great confidence level (if the smoothing is not too extreme).

Higher order statistics ($\langle\kappa^3\rangle$, skewness, $\langle\kappa^4\rangle$, kurtosis, and Minkowski functionals) have higher variances (error bars) in general, and lower discriminating power for the examined models. However, the information obtained from these statistics is precious for its independence from the information offered by statistics such as field variance, and angular power spectrum. It is possible to imagine two cosmological models that have the same mass power spectrum, but different non-Gaussian features. We found that the second Minkowski functional (v_1) is an equal or better model discriminant than the more commonly used third functional (the topological genus), and is very competitive in relation to other measures. This suggests that Minkowski functionals should be included in the row of available statistics to maximally extract information from weak lensing maps. They should be particularly useful to differentiate models that have the same PDF, but distinct morphology.

The presence of noise makes the extraction of information about non-Gaussian features of the pure convergence much more intricate. While for the analyses that are blind to non-Gaussianities (variance and angular power spectrum) the noise term is clearly isolated from the pure convergence term, for analyses sensitive to non-Gaussianities (with exception of $\langle\kappa^3\rangle$) the noise terms are entangled with the pure convergence terms (see equations [24], [29], [B2], and [B5-B7]). So, even for a simple noise model as the one used in our simulations, the modification of the lensing measures due to noise is nontrivial. That implies that the retrieval of information about the pure convergence field (and ultimately, from the underlying large-scale structure and cosmological model) from noisy maps is also nontrivial - even more when the noise field is not well known. Minkowski functionals are a particularly severe example of this entanglement between the pure convergence with noise (as shown in Appendix B).

The complicated analytical description of lensing measures sensitive to non-Gaussian features of noisy maps, and the intrinsic difficulty of incorporating observational aspects trough the analytical approach, favors the use of simulations over an analytical approach for observational predictions, or parameter estimation from real lensing maps. These arguments add to the work of Jain, Seljak & White (2000), which points to the limitations of perturbation theory in providing accurate predictions for most weak lensing statistics at small scales (low smoothing).

Different statistics of weak gravitational lensing maps reveal distinct features of its originating cosmic mass distribution and geometry. Therefore, a comprehensive and realistic study of the underlying cosmological model through weak lensing requires the use of a set of statistics, and the understanding of how these statistics and their variances are affected by observational constraints such as field size and the presence of noise.

ACKNOWLEDGMENTS

I thank Robert Brandenberger for very helpful discussions, and Uroš Seljak for providing codes and valuable knowhow. I also thank the Departments of Physics at Princeton and Rutgers for the use of their facilities during the realization of this work. The research at Brown was supported in part by the US Department of Energy under Contract DE-FG0291ER40688, Task A.

REFERENCES

Bacon, D.J., Refregier, A.R., Ellis, R.S., 2000, MNRAS, 318, 625
Bartelmann, M., Schneider, P., 1999, A&A, 345, 17
Bartelmann, M., Schneider, P., 2001, Phys.Rep., 340, 291
Bernardeau, F., Van Waerbeke, L., Mellier, Y., 1997, A&A, 322, 1
Couchman, H.M.P., Thomas, P.A., Pearce, F.R., 1995, ApJ, 452, 797
Cooray, A., Hu, W., 2001, ApJ, 548, 7
Guimarães, A.C.C., 2001, in Shanks T., Metcalfe N., eds, A New Era in Cosmology, Astronomical Society of the Pacific Conference Series *(to appear)*, astro-ph/0112233
Fischer, P. et al., 2000, ApJ, 120, 1198
Hoekstra, H.,Yee, H., Gladders, M., 2001, astro-ph/0106388
Hui, L., 1999, ApJ, 519, L9
Jain, B., Seljak, U., 1997, ApJ, 484, 560
Jain, B., Seljak, U., White, S., 2000, ApJ, 530, 547
Juszkiewicz, R. et al., 1995, ApJ, 442, 39
Kaiser,N., Squires, G., 1993, ApJ, 404, 441
Kaiser,N., Wilson, G., Luppino,G.A., 2000, astro-ph/0003338
Maoli, R. et al., 2001, A&A, 368, 776
Mellier, Y., 1999, ARA&A, 37, 127
Munshi, D., Jain, B., 2000, MNRAS, 318, 109

Matsubara, T., 2000, preprint (astro-ph/0006269)
Matsubara, T., Jain, B., 2001, ApJ, 552, L89
Rhodes, J., Refregier, A., Groth, E.J., 2001, ApJ, 552, L85
Sato, J., Takada, M., Jing, Y.P., Futamase, T., 2001, ApJ, 551, L5
Van Waerbeke, L., 2000, MNRAS, 313, 524
Van Waerbeke, L. et al., 2000, A&A, 358, 30
Van Waerbeke, L. et al., 2001, A&A. 374, 757
Winitzki, S., Kosowsky, A., 1998, New Astron., 3, 75
Wittman, D.M., Tyson, J.A., Kirkman, D., Dell'Antonio, I., Bernstein, G., 2000, Nature, 405, 143

APPENDIX A: CONSTRUCTION OF THE DIFFERENTIATION

A1 Simple case

Let A and B be models or observations, Y an analysis of lensing maps, and σ^2 its variance. Y_A and Y_B are the result of applying the analysis Y on maps of A and B. Y_A is assumed to follow a normal distribution of mean value $\bar{Y}_A$ and variance σ_A^2

$$F[Y_A] = \frac{1}{\sqrt{2\pi}\sigma_A} e^{-(Y_A-\bar{Y}_A)^2/2\sigma_A^2}. \tag{A1}$$

Equivalently for B.

We define the analysis difference between the two models as

$$D = \frac{Y_A - Y_B}{\sqrt{\sigma_A^2 + \sigma_B^2}}. \tag{A2}$$

It is easy to see that D is a unit normal distribution,

$$F[D] = \frac{1}{\sqrt{2\pi}} e^{-(D-\bar{D})^2/2}, \tag{A3}$$

where the expectation value of D is

$$\bar{D} = \frac{\bar{Y}_A - \bar{Y}_B}{\sqrt{\sigma_A^2 + \sigma_B^2}}. \tag{A4}$$

In fact, we are interested in the absolute value of D, so the distribution function for $|D|$, is

$$\begin{aligned} F[|D|] &= F[D] + F[-D] \\ &= \frac{1}{\sqrt{2\pi}} \left[e^{-(D-\bar{D})^2/2} + e^{-(D+\bar{D})^2/2} \right] . \end{aligned} \tag{A5}$$

If $D = 0$ we say the two models are similar. So the probability of $D = 0$ gives a good measure of how similar the two models are under the analysis Y:

$$F_{|D|}(0) = \sqrt{\frac{2}{\pi}} e^{-\bar{D}^2/2}, \tag{A6}$$

which is normalized to 1 over integration in $\bar{D}$ (from 0 to ∞).

Two very different models ($\bar{D} \gg 0$) have $F_{|D|}(0) \approx 0$; in contrast, two similar models have a large probability that $|D| = 0$. The maximum possible value for $F_{|D|}(0)$ is obtained when $\bar{D} = 0$, which implies

$$\max \left[F_{|D|}(0) \right] = \sqrt{\frac{2}{\pi}} \tag{A7}$$

We can finally define the **differentiation** between the two models under the analysis Y as

$$\mathcal{D}[Y] \equiv 1 - \frac{F_{|D|}(0)}{\max[F_{|D|}(0)]} = 1 - e^{-\bar{D}^2/2}. \tag{A8}$$

A2 Generalization

We can generalize the differentiation for statistics that are functions of a parameter p (e.g. the angular power spectrum as a function of the wavenumber l, or a Minkowski functional as a function of the threshold ν). Note that p, and the analysis itself, can be a vector.

The same elements used before for the simple case can be generalized to $Y_{A,B}(p)$, $\sigma_{A,B}(p)$,

$$D(p) = \frac{|Y_A(p) - Y_B(p)|}{[\sigma_A^2(p) + \sigma_B^2(p)]^{1/2}}. \tag{A9}$$

Using a reasoning similar to the one used in the simple case, we can obtain

$$\mathcal{D}[Y] = 1 - e^{-\chi^2/2}, \tag{A10}$$

where

$$\chi^2 \equiv \left[\int W(p)\,dp\right]^{-1} \int \bar{D}^2(p) W(p)\,dp\,, \tag{A11}$$

and $W(p)$ is a window function (which limits the parameter domain).

Note that the discrete form of χ^2 assumes a very recognizable representation (equation [18]). It becomes then clear that the maximization of $\mathcal{D}[Y]$ is equivalent to the minimization of χ^2, best know as the least square method.

The differentiation can be further generalized to include the effects of covariance by

$$\chi^2 = \frac{1}{N}\sum_{i,j}^{N} [\bar{Y}_A(p_i) - \bar{Y}_B(p_i)](\mathrm{M}^{-1})_{ij}[\bar{Y}_A(p_j) - \bar{Y}_B(p_j)]\,, \tag{A12}$$

where

$$\mathrm{M}_{ij} \equiv \langle [Y_A(p_i) - Y_B(p_i)]\,[Y_A(p_j) - Y_B(p_j)]\rangle \tag{A13}$$

is the covariance matrix, and the brackets denote ensemble average. Note however that we did not include the effects of covariance in our calculations in Section 3.

APPENDIX B: MINKOWSKI FUNCTIONALS OF NOISY MAPS

The problem of expressing the Minkowski functionals for the noisy convergence map κ in terms of the functionals for the pure convergence κ_0 and the smoothed noise n seems to be an open issue. For the first functional, the fractional area, we found a solution, which can be obtained when one makes use of the fact that this functional is the cumulative probability function

$$v_0(\nu) = \int_{\nu\sigma}^{+\infty} F(x)dx\,, \tag{B1}$$

and writes the convergence probability distribution function F_κ as the convolution of F_{κ_0} and F_n (equation [24]), obtaining

$$v_0^{(\kappa)}(\nu) = -\int_{-\infty}^{+\infty} \left[\frac{d}{d\nu'} v_0^{(n)}(\nu')\right] v_0^{(\kappa_0)}\left(\frac{\sigma_\kappa \nu - \sigma_n \nu'}{\sigma_{\kappa_0}}\right) d\nu'\,. \tag{B2}$$

Another approach is to use the approximations (14-16) and calculate how their terms change for a noisy map. In fact, these approximations should be better representations of the noisy map than of the pure map, because noise addition makes the convergence closer to a Gaussian field.

The term $\sigma_1^2 \equiv \langle(\nabla\kappa)^2\rangle$ can be decomposed as

$$\langle(\nabla\kappa)^2\rangle = \langle(\nabla\kappa_0)^2\rangle + \langle(\nabla n)^2\rangle\,, \tag{B3}$$

and it can be useful to note that

$$\langle\nabla\kappa(\boldsymbol{\theta})\nabla\kappa(\boldsymbol{\theta}')\rangle = -C''_\kappa(|\boldsymbol{\theta}' - \boldsymbol{\theta}|)\,, \tag{B4}$$

where $C''_\kappa(r)$ is the second derivative of the two-point correlation function. From (B4) follows that $\langle(\nabla\kappa)^2\rangle = -C''_\kappa(0)$.

The skewness parameters $S_3^{(0)}$ is altered by the addition of noise by

$$S_3^{(0)} = \frac{\langle\kappa^3\rangle}{(\sigma^2_{\kappa_0} + \sigma^2_n)^2}\,, \tag{B5}$$

and to obtain $S_3^{(1)}$ and $S_3^{(2)}$ one needs to calculate

$$\langle\kappa^2(\nabla^2\kappa)\rangle = \langle\kappa_0^2(\nabla^2\kappa_0)\rangle + \langle\kappa_0^2(\nabla^2 n)\rangle + \langle n^2(\nabla^2\kappa_0 + \nabla^2 n)\rangle\,, \tag{B6}$$

$$\langle(\nabla\kappa\cdot\nabla\kappa)(\nabla^2\kappa)\rangle = \langle(\nabla\kappa_0\cdot\nabla\kappa_0)(\nabla^2\kappa_0)\rangle + \langle(2\nabla\kappa_0\cdot\nabla n + \nabla n\cdot\nabla n)(\nabla^2\kappa_0)\rangle + \langle(\nabla\kappa + \nabla n)\cdot(\nabla\kappa + \nabla n)(\nabla^2 n)\rangle\,. \tag{B7}$$

This figure "Fig1.jpg" is available in "jpg" format from:

http://arXiv.org/ps/astro-ph/0202507v1